IEEE Access
Multidisciplinary | Rapid Review | Open Access Journal

Received 10 October 2023, accepted 22 November 2023, date of publication 27 November 2023,
date of current version 5 December 2023.

Digital Object Identifier 10.1109/ACCESS.2023.3337138

RESEARCH ARTICLE

Characterization of LPBF Produced Fe2.9wt.%Si for Electromagnetic Actuator

MICHELE QUERCIO[1], (Member, IEEE), FRANCESCO GALBUSERA[2], EMIR POSKOVIC[1], FAUSTO FRANCHINI[1], LUCA FERRARIS[1], ALDO CANOVA[1], GIAMBATTISTA GRUOSSO[3], (Senior Member, IEEE), ALI GOKHAN DEMIR[2], AND BARBARA PREVITALI[2]

[1]Energy Department, Politecnico di Torino, 10129 Turin, Italy
[2]Department of Mechanical Engineering, Politecnico di Milano, 20156 Milan, Italy
[3]Department of Electronics, Information and Bioengineering, Politecnico di Milano, 20156 Milan, Italy

Corresponding author: Michele Quercio (michele.quercio@polito.it)

This work was supported in part by the Italian Ministry of Education, University and Research through the Project Department of Excellence Lightweight and Smart Structures for Industry 4.0 (LIS4.0); and in part by the European Social Fund (FSE) Recovery Assistance for Cohesion and the Territories of Europe (REACT-EU)—National Operational Program (PON) Ricerca e Innovazione 2014–2020.

ABSTRACT This study aims to produce Fe2.9wt.%Si ferromagnetic material via laser powder bed fusion (L-PBF) for the realization of electromagnetic actuators (EMA). This study is necessary as there are no documents in scientific literature regarding the manufacturing of Iron-Silicon plungers using the L-PBF additive manufacturing (AM) technique. The microstructure, and magnetic properties were characterized using various techniques. The results indicate that the samples produced via L-PBF process exhibit good magnetic properties ($\mu = 748, H_C = 87.7[A/m]$) especially after annealing treatment at 1200° C for 1h ($\mu = 3224, H_C = 69.1[A/m]$), making it a promising material for use in electromagnetic actuators.

INDEX TERMS Actuator, additive manufacturing, electromagnetic plunger, FeSi, laser powder bed fusion, soft magnetic materials.

I. INTRODUCTION

Additive manufacturing, also known as 3D printing, has revolutionized the manufacturing industry by enabling the production of complex geometries and customized parts with high precision and accuracy [1], [2], [3], [4], [5], [6], [7]. One of the most promising additive manufacturing techniques is laser powder bed fusion (LPBF), which involves the use of a high-power laser to selectively melt and fuse metal powder particles layer-by-layer to form a three-dimensional object [8], [9], [10], [11]. The materials used in LPBF can vary depending on the specific application but typically include metals such as titanium, stainless steel, and aluminum [12], [13], [14], [15], [16]. The technique also allows for the production of advanced materials, such as metal matrix composites and high-performance alloys. The potential applications of LPBF are vast and diverse. In aerospace, for example, the technique can be used to produce lightweight components with complex geometries, reducing the weight of aircraft and improving fuel efficiency [17], [18], [19], [20]. In the medical industry, LPBF can be used to produce customized implants and prosthetics with enhanced biocompatibility [21], [22], [23], [24]. In addition, LPBF can be used to produce parts for industrial machinery, consumer electronics, and automotive applications. The ability to produce customized parts with high precision and accuracy can lead to cost savings and reduced lead times in the production process. Overall, using LPBF offers numerous advantages over traditional manufacturing techniques, making it a promising avenue for future research and development in the manufacturing industry [25]. One of the most promising applications of the LPBF technique is in the production of electromagnetic actuators (EMA) [26], [27], [28], which are used in a

The associate editor coordinating the review of this manuscript and approving it for publication was Yangmin Li.

wide range of industrial and consumer applications, such as robotics, aerospace, automotive, and medical devices. EMA require materials with high magnetic permeability, low electrical resistivity, and good mechanical properties. Iron-silicon alloys, such as Fe2.9wt.%Si, have been identified as suitable materials due to their electromagnetic behavior [29]. However, the conventional manufacturing methods for Fe2.9wt.%Si alloys, such as casting and powder metallurgy, must be revised. Despite the potential benefits of LPBF for Fe2.9wt.%Si alloys, there needs to be more research on the ferromagnetic material produced by LPBF. This is a critical gap in knowledge that needs to be addressed to fully realize the potential of LPBF for producing high-performance EMA. Therefore, this study aims to characterize the microstructure and magnetic properties of additively manufactured Fe2.9wt.%Si. The work will also compare the performance of a plunger made by AM in Fe2.9wt.%Si with that of conventionally produced.The comparison took place in terms of closing speed of the system formed by the plug and the electromagnet. In essence, the coil creates a magnetic field with which it attracts the plug inserted inside it which has the possibility of moving and, depending on the application, can either move objects along its axis (that of the coil) or close a device or mechanism. The results of this study will provide valuable insights into the suitability of LPBF for producing Fe2.9wt.%Si alloys for EMA.

II. MATERIALS AND METHODS

This section and figure 1 illustrates the materials, the LPBF architecture and the methodologies used throughout the experimental activity.

A. FESI POWDER

The current study involved the processing of a low alloyed silicon steel powder. The raw material was prepared via powder atomization (m4p material solutions GmbH in Austria). The nominal chemical composition consists of 2.9 wt.% Si and Fe bal. The powder particles presented a spherical morphology, with a granulometry comprised between 20 and 53 μm.

B. LPBF SYSTEM

To conduct magnetic characterization, samples were produced using a semi industrial LPBF system with open architecture (LLA150R, 3D-NT, Solbiate Olona, Italy). The system utilizes a multi-core fiber laser source with dynamic beam shaping capabilities (Corona nLIGHT AFX 1000, nLIGHT Inc, Vancouver, Washington, USA). The laser source emits at a wavelength of 1070 nm ($\pm$10 *nm*), either in Pulsed Wave (PW) or Continuous Wave (CW) regimes of power modulation, and provides a maximum power of 600 W, with a common Gaussian power density distribution, up to 1.2 kW with other novel ring-like profiles. The LPBF system features an optical architecture made of a collimating lens at the fiber end, reflective mirrors for the beam propagation, a scanning head for the beam manipulation, and an f-Theta

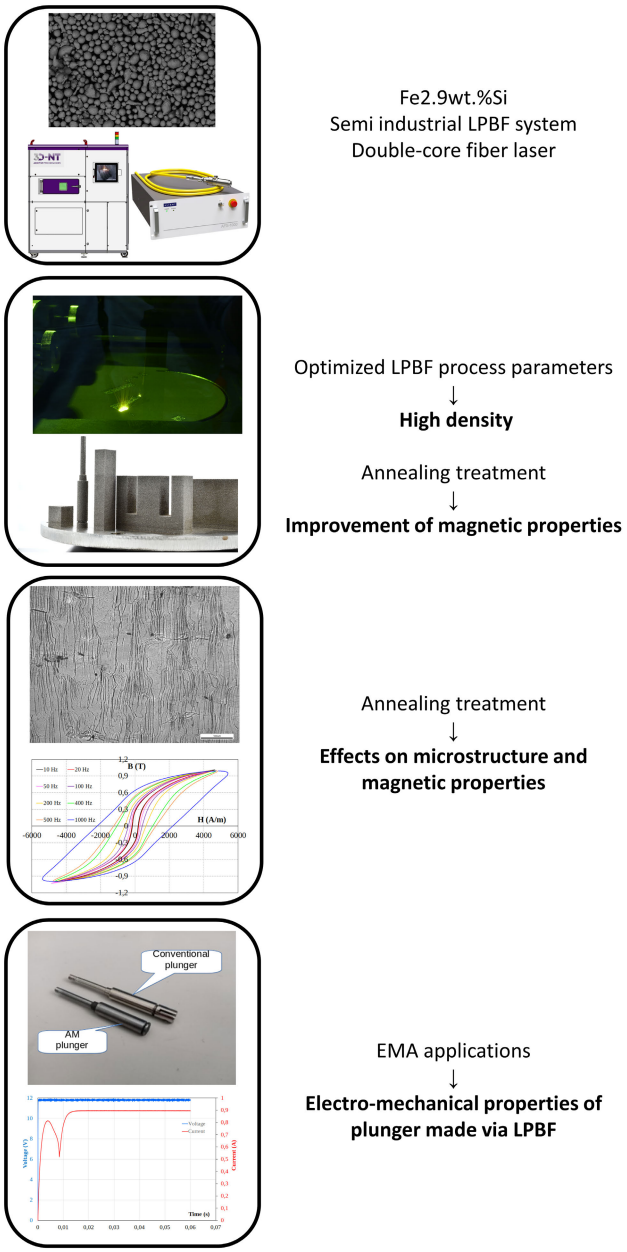

FIGURE 1. Flowchart describing the steps's project.

lens to focus the laser beam onto the substrate. This optical configuration can guarantee a minimum laser beam diameter of 47 μm when operating with a conventional Gaussian distribution of power. Prior to LPBF processing, the building chamber is filled with Ar in over pressure while keeping the O_2 content below 3000 ppm. Ferromagnetic samples were built on commercial stainless steel substrates during the experiment and detached with an automatic linear sawing to prevent undesired deformation.

C. PRODUCTION OF COMPONENTS

3D sample models were designed and sliced with CAD softwares. The height of each slice corresponds to a layer

of powder deposited during the LPBF process, which is commonly called layer thickness (z). Using a CW regime of power modulation, the focused laser beam scanned and melted the metallic powder following a bidirectional pattern (“zig zag”), at a fixed average power (P) and scan speed (v). The hatch was defined by consecutive lines equally spaced of the hatch distance (h_d), and layer-by-layer was also rotated by an angle (α) of 67°. The graphical schematisation of the LPBF process and the main parameters are depicted in fig. 2 a. The growing direction of the parts was aligned with their main axis, except for the toroid, which was directed vertically. To ensure highly dense samples (> 99.9%), a preliminary experimentation was conducted to determine the best process parameters. The optimized process parameters used throughout the LPBF process are listed in Table 1. Table 2 shows the sample types, including their close view, size, and function while fig. 2 b illustrates an overview of the 3D samples attached to the substrate after building.

TABLE 1. List of optimum process parameters used to produce highly dense samples.

Process parameters	Value
Laser power, P(W)	200
Scan speed, v(mm/s)	800
Hatch distance, $h_d(\mu m)$	70
Layer thickness, z(μm)	30
Hatching rotation, $\alpha(^\circ)$	67
Inert Gas type	Ar
Power emission mode	CW
Substrate material	AISI 316L

TABLE 2. List of specifications for the samples built via LPBF.

Sample	Close view	Size	Function
Cube		a=10 mm	Microstructure characterization
Rod1	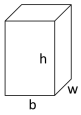	b=3mm w=5mm h=10mm	Coercitivity measurements
Rod2	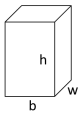	b=5mm w=5mm h=10mm	Coercitivity measurements
Toroid	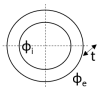	$\phi_i = 10$mm $\phi_o = 13$mm t=2mm	Magnetic permeability Specific iron losses Magnetization curves Hysteresis cycles
Plunger	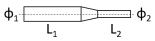	$\phi_1 = 6$mm $\phi_2 = 4$mm $L_1 = 25$mm $L_2 = 21$mm	Coercitivity measurements Closing device application

After detaching the components from the substrate and removing additional support structures, an annealing

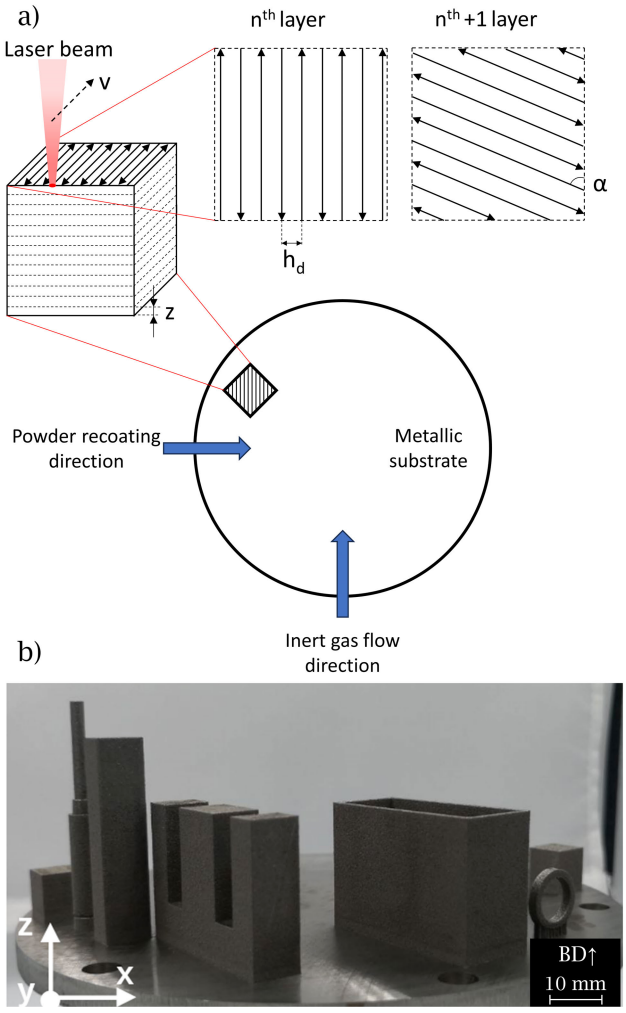

FIGURE 2. a) Schematisation of LPBF process with details of the powder recoating and the inert gas flow directions. “v” is the scan speed, “z” is the layer thickness, “h_d” is the hatch distance and “α” is the hatching rotation angle. b) Overview of the 3D samples made of Fe2.9wt.%Si via LPBF.

treatment was performed to achieve satisfactory magnetic performance. The thermal treatment included heating the samples at a constant temperature of 1200°C for 1 hour under vacuum, as recommended from the literature [30]. To unravel the effect of the thermal treatment on the microstructure, some micrographs were collected before and after the annealing by applying conventional metallographic procedures on sacrificial bulky cubes. Nital 2% reagent was used to etch the microstructure. From the micrographs, grain size measurements were performed in terms of grain width (w) and height (h). Accordingly, the grain Aspect Ratio (AR) was calculated as a quantitative indicator of grain morphology:

$$AR = \frac{h}{w} \tag{1}$$

Definition of grain morphology based on AR is well-known in the literature. Usually, according to the previous definition,

an AR less than 2 is the threshold for a fully equiaxed grain structure [31]. AR measurements were taken to provide a quantitative insight about the annealing effect on grain morphology.

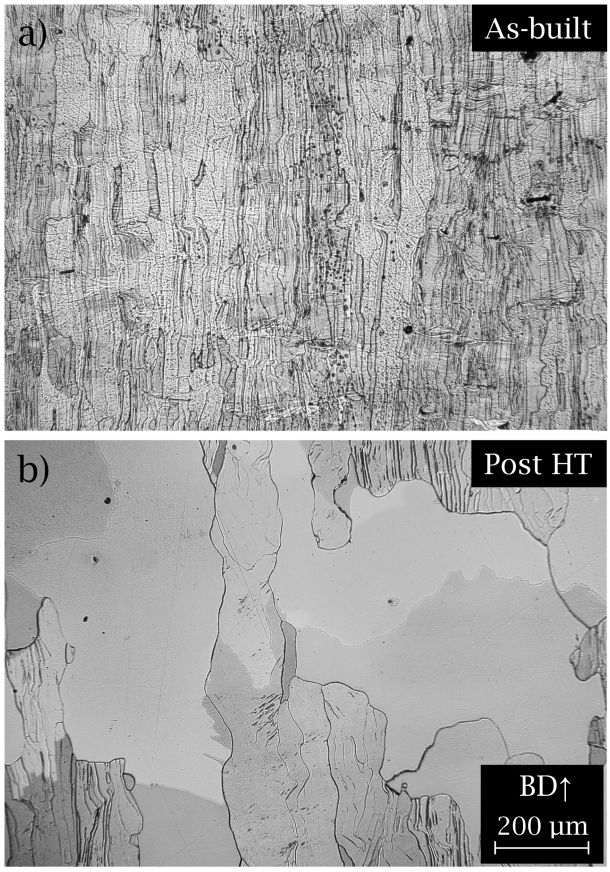

FIGURE 3. LPBF produced FeSi2.9 microstructure a) in as-built condition and b) after heat treatment at 1200°C.

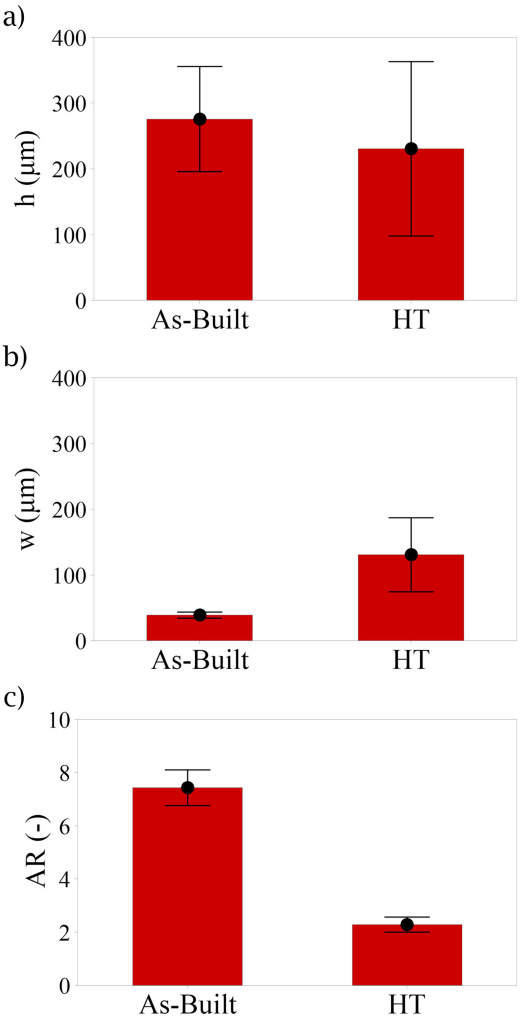

FIGURE 4. Comparison between as-built and heat treated (HT) condition in terms of a) grain height (h), b) grain width (w) and c) aspect ratio (AR). Interval bars are defined based on standard errors.

III. MICROSTRUCTURE CHARACTERIZATION

Figure 3 a-b depicts the microstructure before and after annealing, respectively. Fig. 3 a shows that the revealed microstructure is dominated by columnar and elongated grains along the build direction (BD). At high magnifications, melt pool boundaries can also appear but not sufficiently to extract geometrical insight. Conversely, as appears from Fig. 3 b, the annealed microstructure is made of coarser and larger grains, mixed with smaller columnar grains, still stretched towards the build direction. The effect of annealing treatment promotes grain growth and coarsening, thus significantly reducing the grain boundaries within the volume. This is believed to influence magnetic domains since grain boundaries might act as pin walls for them. Nonetheless, as appears from fig. 3 b, the resultant microstructure after annealing is still featured by residual columnar and elongated grains typical of the as-built conditions and primarily located in the periphery of the coarser grains. This may suggest that the annealing treatment can be further optimized to control the microstructure, i.e., removing the smaller columnar grains, homogenizing the microstructure, and thus enhancing the magnetic properties. A quantitative proof of the annealing treatment on the microstructure is provided in fig. 4. Hereby, the comparison between measured height, width and aspect ratio. As the graphs show, the annealed microstructure is featured by wider rather than higher grains if compared to the as-built condition. This leads to a reduction of grain AR, from 7.4 to 2.3 (mean values) after annealing. Considering that a grain AR of 2 is considered as a threshold for discriminating between columnar and equiaxed grain morphology [31], and that the significant effect induced from annealing is the reduction of AR towards grain equiaxity, it can be concluded that the microstructure plays a crucial role in the determination of magnetic properties.

IV. MAGNETIC CHARACTERIZATION

The magnetic properties of produced components are detected to understand the possible relevant applications. Coercivity measurement and toroidal magnetic test are used

to identify magnetic and energetic behavior. Also, the Single Sheet Tester (SST) can be applied, but the specimens require very high planarity. The procedure is more similar to the characterization of bulk or Soft Magnetic Composite (SMC) materials instead of laminated steel [32].

A. COERCIVITY MEASUREMENT

A rapid and dependable method can effectively demonstrate the impact of heat treatment on magnetic hysteresis. The Hc value, measured in a slow transient, is closely linked to the hysteresis cycle's area. The coercimeter used consists of a controlled power supply, an excitation coil, and two sensing coils (fig. 5)). The maximum magnetic field value during the saturation phase is 100 kA/m, and the Hc point is reached within 10 seconds, which reduces most of the eddy current contribution. Table 3 confirms the anticipated material behavior, indicating a significant reduction in residual stresses due to the fast cooling cycles induced in the LPBF process. The plunger exhibited a low coercivity value even before treatment, which requires further investigation as it may be related to the specimen's shape or printing conditions for such a small diameter. This measurement is highly advantageous for indicating hysteresis losses, mainly when dealing with multiple samples under different conditions, such as temperature treatment effects. For example, some soft magnetic material families limit Hc values to 500 A/m; higher values are not considered for further characterization and analysis, saving time and materials.

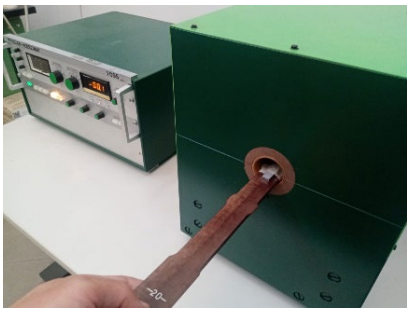

FIGURE 5. Specimen insertion in the coercimeter coil.

TABLE 3. Coercivity values before and after thermal treatment.

Sample	No treatment(A/m)	Treatment at 1200°C in vacuum(A/m)
Rod1	151.6	94.6
Rod2	212	85.6
Plunger	87.7	69.1

B. TOROIDAL MAGNETIC TEST

The soft material hysteresis graph was tested at 10 Hz and 1 kHz frequencies. The measurements were limited to an excitation field peak of 6500 A/m, or a secondary voltage peak of 10 V. The toroidal sample had two windings:

FIGURE 6. FeSi2.9 Toroid: size and shape not fully compliant with the IEC 60404 series standards.

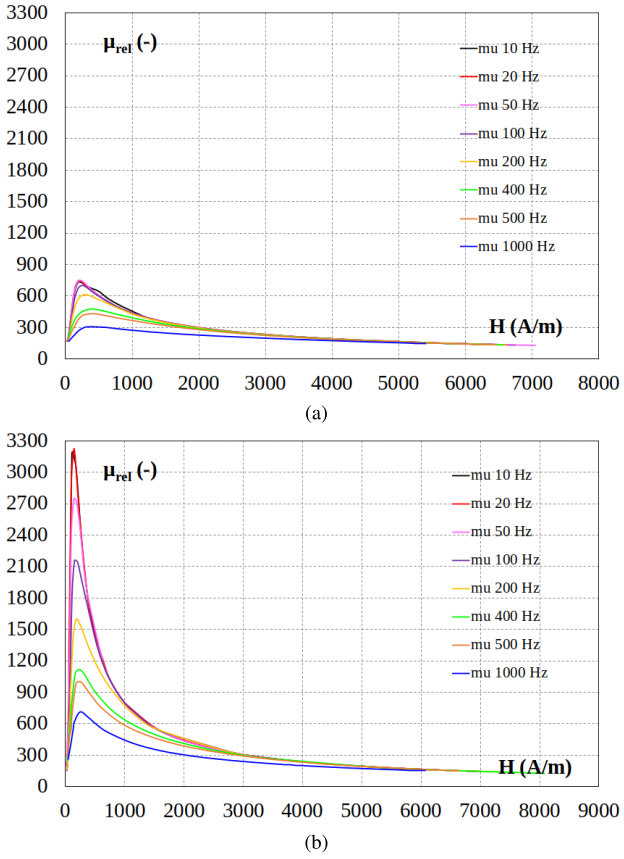

FIGURE 7. Magnetic permeability as a function of magnetic field H at different frequencies for FeSi2.9 toroid a) without and b) with heat treatment at 1200°C.

a secondary one($N_2 = 145$), thinner, directly on the sample surface and a primary one ($N_1 = 134$) on top of the former (as shown in Figure 6). The geometrical sizes are: full square section of 5 mm side, 5 cm inner diameter and 6 cm outer diameter. The wrapped specimen was used for typical magnetic characterization performed with the transformer approach. The harmonic content had to be very low for a sinusoidal waveform, and the equipped arrangements guaranteed a Total Harmonic Distortion (THD) lower than 1%. The data acquisition system was prepared with a dedicated LabView code to automatically acquire and process data for calculating the magnetic and energetic properties. The comparison between the measurements conducted before and after the heat treatment showed different material properties and helped to adjust the next steps of the research activities. The main differences were in the

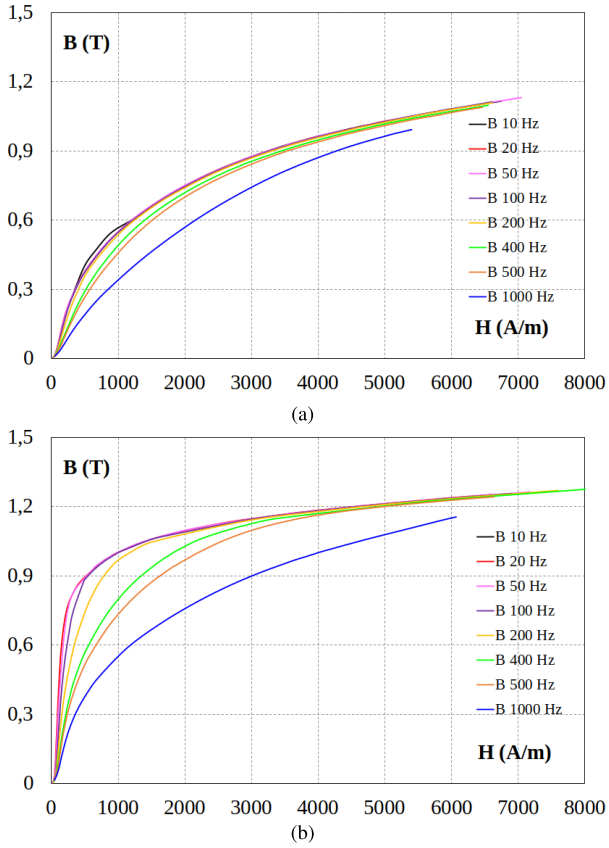

FIGURE 8. Magnetization curves at different frequencies for FeSi2.9 toroid a) without and b) with heat treatment at 1200°C.

maximum magnetic permeability and total iron losses. The magnetic permeability before the heat treatment was lower than expected for the adopted powder composition (as shown in figure 7a), mainly indicating a poorly relaxed state of the crystal lattices. Consequently, the magnetization curves were close to different frequencies (as shown in figure 8a) and they all show very low maximum values for the alloy considered. The maximum magnetic permeability value was 748, and magnetic induction did not exceed 1.1 T without the heat treatment. The iron losses measured before the heat treatment showed a relatively low electrical resistivity, with the complete cycles at 1 T losing their tips, but only at 500 Hz and 1 kHz. The hysteresis contribution was still relatively high at all frequencies (as shown in figure 10). The magnetic permeability rises consistently after the heat treatment (fig. 7b), bringing the hysteresis contribution to the iron losses at shallow levels. The maximum magnetic permeability after the treatment corresponds to 3224, and magnetic induction shows values greater than 1.2 T (fig. 8b). The total iron losses after the heat treatment surprisingly decreased at all frequencies and for any peak induction value, as reported in Fig. 9, showing that the heat treatment benefits fully compensate for the reduction in global electrical resistivity. The hysteresis cycles before the treatment are reported in Fig. 10a; it is possible to note the high presence of total losses. The complete cycles at 1 T show a strongly

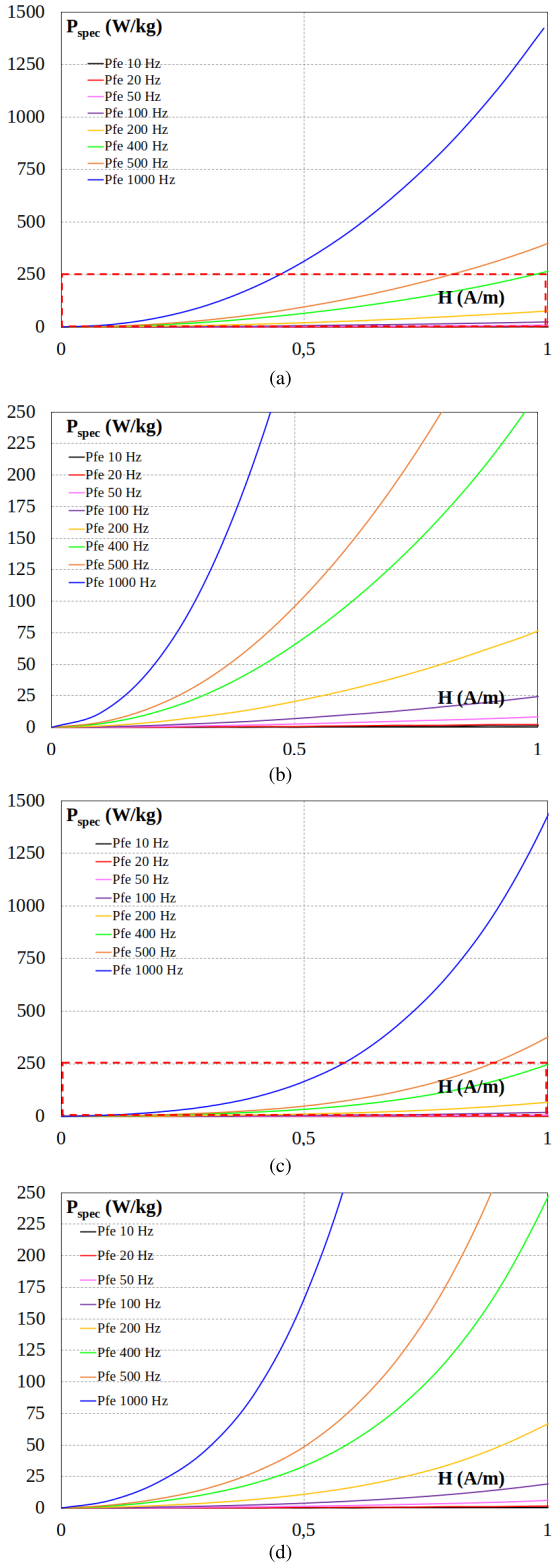

FIGURE 9. Specific iron losses as a function of magnetic induction at different frequencies for FeSi2.9 toroid a) without heat treatment, b) without heat treatment restricted to 250 W/kg,c) with heat treatment at 1200°C, and d) with heat treatment at 1200°C restricted to 250 W/kg.

reduced electrical resistivity, typical of a fully sintered internal structure (fig. 10b), in which the central part of

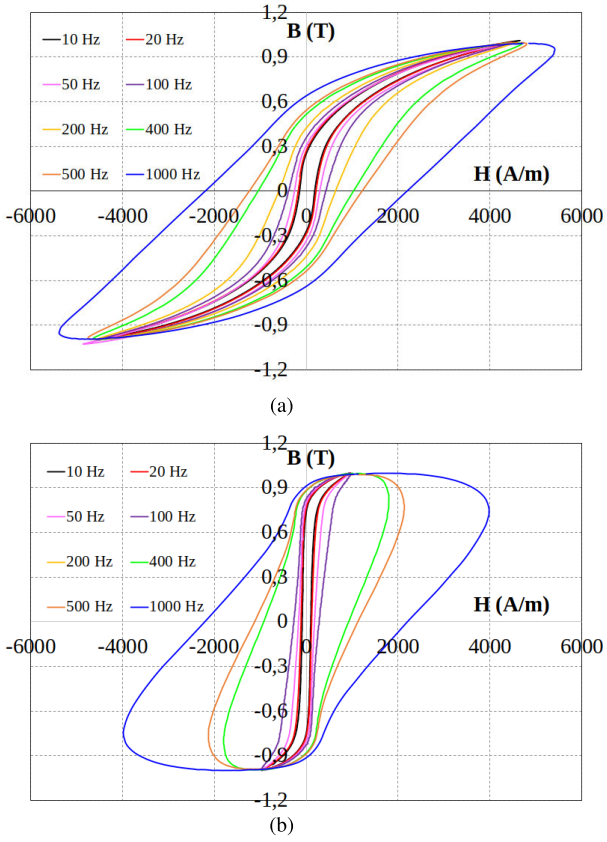

FIGURE 10. Hysteresis cycles at different frequencies for FeSi2.9 toroid a) without treatment and b) with heat treatment at 1200°C.

the iron losses is dynamic and originates from the eddy currents. The typical cycle shape confirms the resistivity reduction for increasing frequencies; the cycle shape tends to be an ellipsoid. On the other hand, the hysteresis losses are reduced, as demonstrated by the minor Hc values at very low frequencies; however, the contribution of eddy currents losses became more influential after thermal treatment. The separation of iron losses can be interpreted through the specific lost energy shown in fig.11; the hysteresis part is halved after the thermal treatment, while the eddy currents losses show a slight increment. The additional investigation concerns the maximum magnetic permeability as the function of the frequency, as shown in Fig. 12a. The reduction is more pronounced after the heat treatment, and at 100 Hz, the reached value is 50% compared to the maximum. A similar percentage decrease is obtained at 400 Hz for no heat treatment (fig. 12a). The iron losses @1T for various frequencies are shown in Fig. 12b. As it appears, irrespective of the tested frequencies, the specific iron losses show a slight decrease as an effect of annealing, suggesting that the significant role of the heat treatment is played on the magnetic permeability. So, the microstructure thus plays a crucial role in controlling the magnetic properties, as appears from the significant increase of magnetic permeability, the slight reduction of specific iron losses, and the coercitivity reduction.

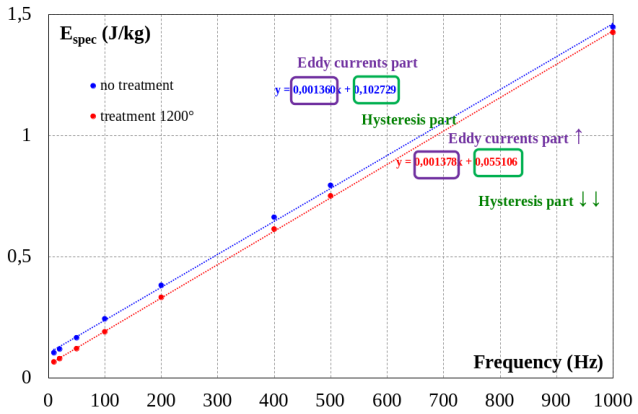

FIGURE 11. Separation of hysteresis and eddy current specific lost energy; the hysteresis part decreases significantly (-54%) while the eddy currents part increases slightly (1.32%) after the thermal treatment.

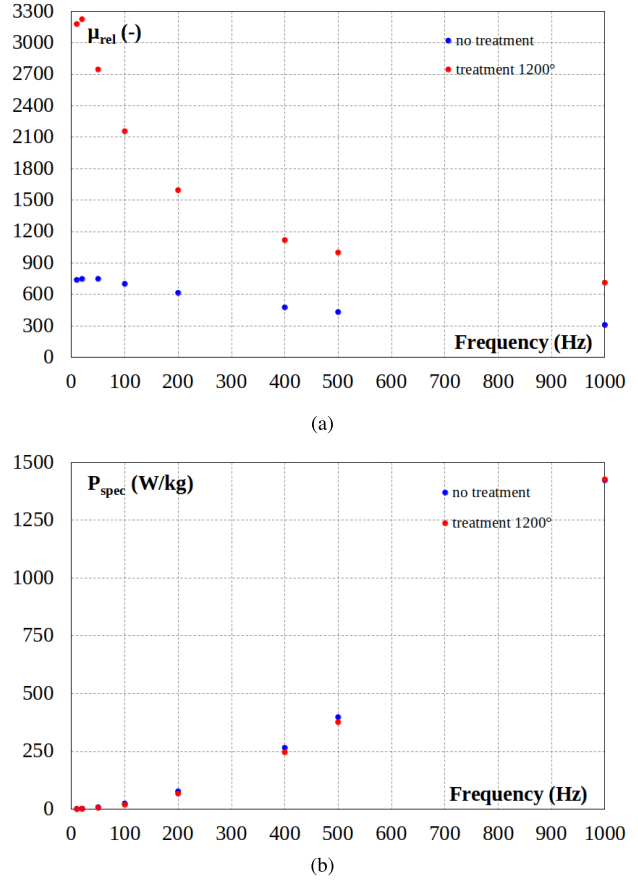

FIGURE 12. a) Comparison between magnetic permeability before and after thermal treatment as a function of frequency. b) Comparison between specific iron losses before and after thermal treatment as a function of frequency.

V. NUMERICAL SIMULATION

The plunger is a movable ferromagnetic core that is driven by an electromagnetic force generated by a coil. The design of the plunger is critical to ensure efficient and reliable operation of the device. Numerical simulation is a powerful tool that can be used to optimize the design of the plunger and predict

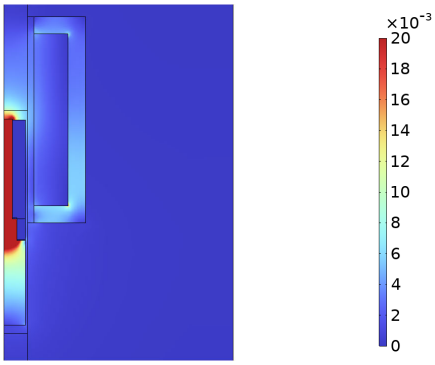

FIGURE 13. Simulation of the plunger as it passes through the electromagnet.

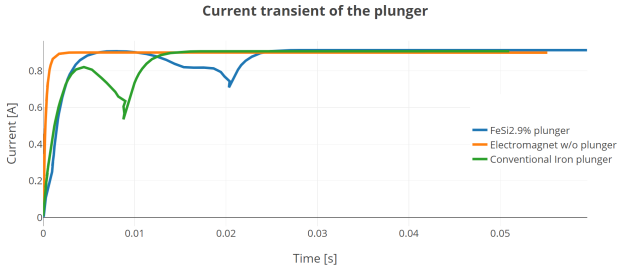

FIGURE 14. Simulation data of the current transient of the plunger under different condition. Orange) electromagnet only, Green) conventional iron plunger, Blue) FeSi2.9% plunger.

its performance characteristics. This section will discuss the numerical simulation of the linear electromagnetic plunger produced by the LPBF technique. The magnetic field can be calculated using the Maxwell's equations. The equations can be solved numerically using finite element analysis (FEA) software such as COMSOL Multiphysics. The FEA software discretizes the geometry into small elements and solves the equations for each element. The results are then combined to obtain the overall solution. The simulation setup includes the geometry of the plunger, the material properties, and the boundary conditions. The geometry of the plunger was created using COMSOL Multiphysics fig. 13. The material properties inserted in the simulation come from the measured data obtained experimentally. The boundary conditions include the current flowing through the coil and the external magnetic field. The simulation results provide valuable insights into the performance characteristics of the plunger, the curve in Fig. 14 shows the current transient of the plunger. What can be seen from the trends is that in the case of the plug produced by AM (blue line) there is a delay in closing of 10 ms compared to the traditional case. This phenomenon is due to a longer time constant than the current transient. The peaks at the bottom represent the moment in which the electromagnet's thrusts reach the end of their stroke, while the following segment represents the time in which the system reaches steady state. The simulation results can also be used to calculate the magnetic flux density distribution in the plunger(fig. 13). The distribution shows

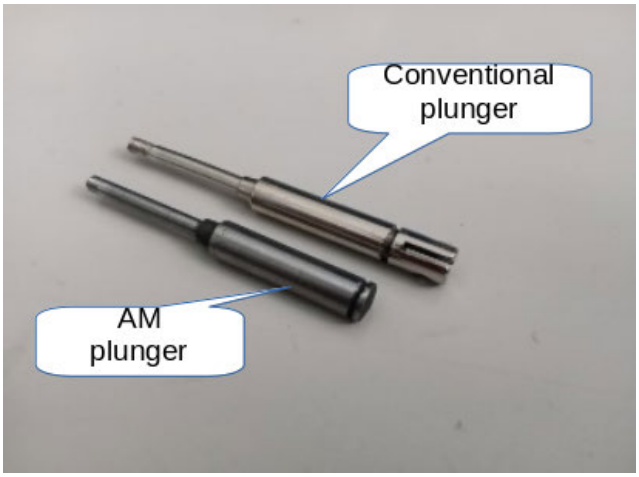

FIGURE 15. Conventionally manufactured and LPBF produced plunger.

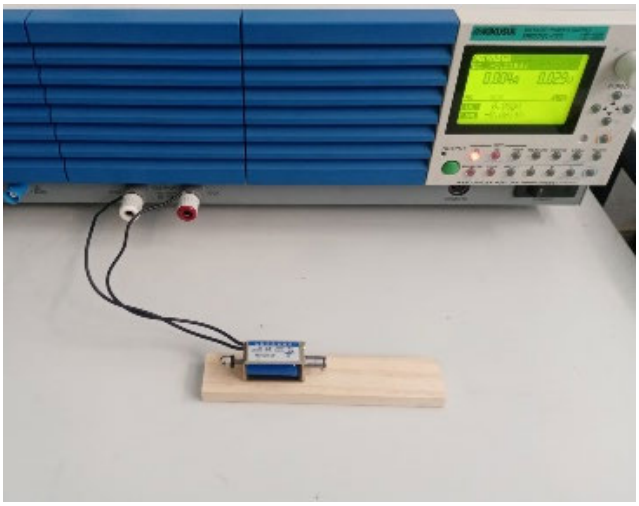

FIGURE 16. Setup for plunger closing measurenments.

how the magnetic field is distributed in the plunger and can be used to identify areas of high flux density that may cause saturation or heating. The results can also be used to optimize the design of the coil to ensure uniform distribution of the magnetic field.

VI. LABORATORY EXPERIMENT

One of the produced FeSi samples fits as the cursor in a small magnetic piston. This device is based on a coil, magnetically pulling an inner solid cursor. The used model is of the single effect type, thus including a counteracting spring. The nominal voltage of the device is 12 Vdc. Despite the restrained sizes of the plunger and the setup, this application could be considered an in-house demonstrator for locking devices (e.g., for doors, electromechanical valves, etc.). After the LPBF process, the sample needed to be machined to obtain smooth surfaces and the thread for the end damper and nut. The tests on the device with the original and the newly produced rods, shown in Fig. 15, led to a direct

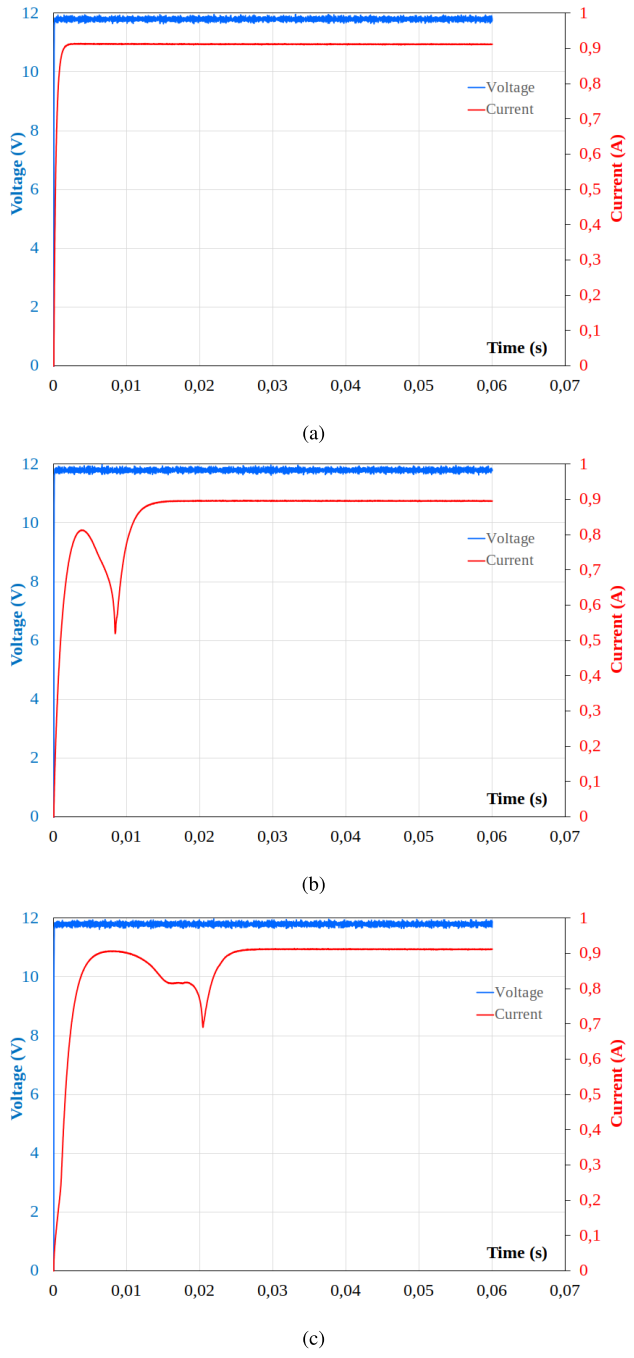

FIGURE 17. Initial current transient.: a) Solenoid only, b) conventionally manufactured small plunger, c) LPBR produced small plunger.

electrical and mechanical comparison between the materials. During the tests, a voltage step at the nominal level (12Vcd) caused the cursor movement until the natural stop position (figure 16). The recorded voltage and current waveforms are shown in fig.17. This test allows to evaluate the closing transient of the plug and therefore its performance through current measurement. The peak located at the instant 0.01 s in fig. 17b, and 0.02 s in case fig. 17c represents the instant in which the plug has reached the point of maximum closure for which the system formed by the coil and the ferromagnetic core begins to reach steady state according to the exponential law typical of inductive components. The dimensions of the two plungers were slightly different. Indeed, the as-built sample was broader owing to the optimized LPBF process tolerances and shorter than the standard one. Hence, the setup and the initial cursor position were adjusted in the two cases to provide the same total stroke of 10 mm.

In the first transient test, the coil had no cursor inside, so only the electrical contribution to the current transient is visible (fig. 17a). The presence of the cursor in the second and third tests changed the current waveform (fig. 17b-c), clearly showing the cursor travel phase and the time the movement was completed. The latter can be easily detected as the last current slope inversion, after which the current completes the exponential transient following the higher final inductance value. The main result that appears from Fig. 17 is that the lower force acting on the FeSi rod causes a reduced acceleration (fig. 17c), with a longer travel time of about 10 ms concerning the original rod (fig. 17b). Future improvements to the test bench could lead to the measurement of the transient speed trend or the force acting on the cursor at different positions.

VII. CONCLUSION

This work investigated the LPBF processability and functional characterization of soft magnetic FeSi2.9 specimens. Magnetic permeability, coercitivity, first magnetization curves, specific power losses, and hysteresis cycles were measured at different operating frequencies (10 Hz-1000 Hz) before and after a non-standard annealing heat treatment (1200°C under vacuum for 1hr), to match the performances of conventionally manufactured silicon steels. Additional microstructure and grain size characterization were conducted to clarify the effect of annealing treatment on magnetic properties. The overall results can be summarized as follows:

- Annealing heat treatment allowed a significant alteration in the microstructure of the specimens, passing from the columnar and elongated grains for the as-built condition to larger and coarser grains for the heat-treated one. Additional grain size measurement regarding grain aspect ratio revealed that the attempted heat treatment fosters the formation of equiaxed grains.
- LPBF processability does not match the functional properties required from soft magnetic FeSi2.9. Post-annealing heat treatment is required to match the magnetic performances.
- Magnetic permeability is the magnetic properties that annealing influences the most. After annealing, $\mu_{rel} >$ 2700 is reached at 50Hz and higher than 3000 for lower frequencies. On the contrary, specific power loss measurements revealed only a tiny reduction trend due to annealing for each tested frequency.

- Annealing heat treatment allowed for significantly dampening the hysteresis losses at each tested frequency, showing that the dominant part of iron losses originates from eddy currents.
- A simple cursor demonstrator for locking device applications was successfully built, tested with the proper electromagnetic induction circuit, and compared with a conventional plunger. The result of the test shows that the FeSi plunger showed a higher travel time to cover the same stroke as an effect of a reduced force acting on it. Ultimately, the chosen application is consistent with the magnetic and energetic material characteristics, which are unsuitable for magnetic cores that work with alternating magnitudes.

This work demonstrates great potentialities enabled by the LPBF process in manufacturing soft magnetic Fe2.9wt.%Si. Post-annealing treatment is a mandatory technological step to attain adequate magnetic properties. Moreover, this work also demonstrates that the microstructure rules magnetic properties. Optimal magnetic properties are achieved when the microstructure comprises large equiaxed grains. Otherwise, even if the eddy current losses are high, the magnetic aspect is comparable to ferromagnetic materials produced by powder metallurgy. Some applications are already possible for very low frequencies. Moreover, other solutions can be investigated in the future, such as the stator for axial flux machines [33] and the rotor for synchronous axial reluctance machines. Therefore, further works will focus on reducing eddy current loss strategies, for instance, by acting on the geometry of the specimens. Another essential action will be to study the increment in Si content, one of the most important characteristics of the additive manufacturing of magnetic components that can be exploited, as described in several papers, and the evaluation of the force.

ACKNOWLEDGMENT

The part of research activities developed by Emir Poskovic was carried out within the Ministerial Decree no. 1062/2021. This manuscript reflects only the authors' views and opinions, neither the European Union nor the European Commission can be considered responsible for them.

REFERENCES

[1] B. H. Jared, M. A. Aguilo, L. L. Beghini, B. L. Boyce, B. W. Clark, A. Cook, B. J. Kaehr, and J. Robbins, "Additive manufacturing: Toward holistic design," *Scripta Mater.*, vol. 135, pp. 141–147, Jul. 2017.

[2] M. Vaezi, S. Chianrabutra, B. Mellor, and S. Yang, "Multiple material additive manufacturing—Part 1: A review: This review paper covers a decade of research on multiple material additive manufacturing technologies which can produce complex geometry parts with different materials," *Virtual Phys. Prototyping*, vol. 8, no. 1, pp. 19–50, Mar. 2013.

[3] J. Gardan, "Additive manufacturing technologies: State of the art and trends," in *Additive Manufacturing Handbook*, 1st ed. New York, NY, USA: Taylor & Francis, 2017, pp. 149–168.

[4] U. M. Dilberoglu, B. Gharehpapagh, U. Yaman, and M. Dolen, "The role of additive manufacturing in the era of Industry 4.0," *Proc. Manuf.*, vol. 11, pp. 545–554, Dec. 2017.

[5] A. Canova, G. Gruosso, and M. Quercio, "Characterization of electromagnetic device by means of spice models," *Int. J. Emerg. Technol. Adv. Eng.*, vol. 11, no. 9, pp. 12–22, Sep. 2021. [Online]. Available: https://ijetae.com/files/Volume11Issue9/IJETAE092102.pdf

[6] S. Guo, C. Hu, and H. Zhang, "Unidirectional ultrabroadband and wide-angle absorption in graphene-embedded photonic crystals with the cascading structure comprising the Octonacci sequence," *J. Opt. Soc. Amer. B, Opt. Phys.*, vol. 37, no. 9, p. 2678, Sep. 2020. [Online]. Available: https://opg.optica.org/josab/abstract.cfm?URI=josab-37-9-2678

[7] S. Liao, Z. Qiao, J. Sui, and H. Zhang, "Multifunctional device for circular to linear polarization conversion and absorption," *Annalen der Physik*, vol. 535, no. 7, Jul. 2023, Art. no. 2300195. [Online]. Available: https://onlinelibrary.wiley.com/doi/abs/10.1002/andp.202300195

[8] S. L. Sing, C. N. Kuo, C. T. Shih, C. C. Ho, and C. K. Chua, "Perspectives of using machine learning in laser powder bed fusion for metal additive manufacturing," *Virtual Phys. Prototyping*, vol. 16, no. 3, pp. 372–386, May 2021, doi: 10.1080/17452759.2021.1944229.

[9] I. Yadroitsev, I. Yadroitsava, A. Du Plessis, and E. MacDonald, *Fundamentals of Laser Powder Bed Fusion of Metals*. Amsterdam, The Netherlands: Elsevier, 2021.

[10] S. Kumar, "Laser powder bed fusion," in *Additive Manufacturing Processes*. Cham, Switzerland: Springer, 2020, pp. 41–63.

[11] M. Khorasani, I. Gibson, A. H. Ghasemi, E. Hadavi, and B. Rolfe, "Laser subtractive and laser powder bed fusion of metals: Review of process and production features," *Rapid Prototyping J.*, vol. 29, no. 5, pp. 935–958, May 2023.

[12] W. E. King, A. T. Anderson, R. M. Ferencz, N. E. Hodge, C. Kamath, S. A. Khairallah, and A. M. Rubenchik, "Laser powder bed fusion additive manufacturing of metals; physics, computational, and materials challenges," *Appl. Phys. Rev.*, vol. 2, no. 4, Dec. 2015, Art. no. 041304.

[13] J. P. Oliveira, A. D. Lalonde, and J. Ma, "Processing parameters in laser powder bed fusion metal additive manufacturing," *Mater. Design*, vol. 193, Aug. 2020, Art. no. 108762.

[14] E. Santecchia, S. Spigarelli, and M. Cabibbo, "Material reuse in laser powder bed fusion: Side effects of the laser—Metal powder interaction," *Metals*, vol. 10, no. 3, p. 341, Mar. 2020.

[15] M. A. Obeidi, "Metal additive manufacturing by laser-powder bed fusion: Guidelines for process optimisation," *Results Eng.*, vol. 15, Sep. 2022, Art. no. 100473.

[16] A. Khorasani, I. Gibson, J. K. Veetil, and A. H. Ghasemi, "A review of technological improvements in laser-based powder bed fusion of metal printers," *Int. J. Adv. Manuf. Technol.*, vol. 108, nos. 1–2, pp. 191–209, May 2020.

[17] D. W. Gibbons, J.-P.-L. Serfontein, and A. F. van der Merwe, "Mapping the path to certification of metal laser powder bed fusion for aerospace applications," *Rapid Prototyping J.*, vol. 27, no. 2, pp. 355–361, Mar. 2021.

[18] H. Hilal, R. Lancaster, S. Jeffs, J. Boswell, D. Stapleton, and G. Baxter, "The influence of process parameters and build orientation on the creep behaviour of a laser powder bed fused ni-based superalloy for aerospace applications," *Materials*, vol. 12, no. 9, p. 1390, Apr. 2019.

[19] A. S. Metel, S. N. Grigoriev, T. V. Tarasova, A. A. Filatova, S. K. Sundukov, M. A. Volosova, A. A. Okunkova, Y. A. Melnik, and P. A. Podrabinnik, "Influence of postprocessing on wear resistance of aerospace steel parts produced by laser powder bed fusion," *Technologies*, vol. 8, no. 4, p. 73, Dec. 2020.

[20] A. C. R. Marques, Ó. S. N. Carvalho, F. S. Silva, F. Bartolomeu, S. Pereira, and P. Alexandrino, "Inconel 718—Copper bimetallic joints fabricated by 3D multi-material laser powder bed fusion for aerospace components," Universidade do Minho, Braga, Portugal, Tech. Rep. 21, 2023.

[21] S. Huang, S. L. Sing, G. de Looze, R. Wilson, and W. Y. Yeong, "Laser powder bed fusion of titanium-tantalum alloys: Compositions and designs for biomedical applications," *J. Mech. Behav. Biomed. Mater.*, vol. 108, Aug. 2020, Art. no. 103775.

[22] I. Yadroitsev, P. Krakhmalev, I. Yadroitsava, and A. Du Plessis, "Qualification of Ti6Al4V ELI alloy produced by laser powder bed fusion for biomedical applications," *J. Oper. Manag.*, vol. 70, no. 3, pp. 372–377, Mar. 2018.

[23] A. Jam, A. du Plessis, C. Lora, S. Raghavendra, M. Pellizzari, and M. Benedetti, "Manufacturability of lattice structures fabricated by laser powder bed fusion: A novel biomedical application of the beta Ti-21S alloy," *Additive Manuf.*, vol. 50, Feb. 2022, Art. no. 102556.

[24] M. L. Gatto, A. Santoni, E. Santecchia, S. Spigarelli, F. Fiori, P. Mengucci, and M. Cabibbo, "The potential of duplex stainless steel processed by laser powder bed fusion for biomedical applications: A review," *Metals*, vol. 13, no. 5, p. 949, May 2023.

[25] M. Quercio, F. Galbusera, A. Canova, A. G. Demir, G. Gruosso, and B. Previtali, "Electromagnetic shielding properties of LPBF produced Fe2.9wt.%Si alloy," *J. Phys., Energy*, vol. 5, no. 4, Oct. 2023, Art. no. 045003. [Online]. Available: http://iopscience.iop.org/article/10.1088/2515-7655/ace92f
[26] V. Laitinen, "Laser powder bed fusion for the manufacture of Ni-Mn-Ga magnetic shape memory alloy actuators," Tech. Rep., 2021.
[27] D. Wang, J. Wang, Z. Shen, C. Jiang, J. Zou, L. Dong, N. X. Fang, and G. Gu, "Soft actuators and robots enabled by additive manufacturing," *Annu. Rev. Control, Robot., Auto. Syst.*, vol. 6, no. 1, pp. 31–63, May 2023.
[28] M. Manns, J. Morales, and P. Frohn, "Additive manufacturing of silicon based PneuNets as soft robotic actuators," *Proc. CIRP*, vol. 72, pp. 328–333, Jun. 2018.
[29] M. Quercio, F. Galbusera, E. Pošković, F. Franchini, L. Ferraris, A. Canova, G. Gruosso, A. G. Demir, and B. Previtali, "Functional characterization of L-PBF produced FeSi2.9 soft magnetic material," in *Proc. Int. Conf. Electr. Mach. (ICEM)*, Sep. 2022, pp. 531–537.
[30] M. Garibaldi, I. Ashcroft, J. N. Lemke, M. Simonelli, and R. Hague, "Effect of annealing on the microstructure and magnetic properties of soft magnetic Fe-Si produced via laser additive manufacturing," *Scripta Mater.*, vol. 142, pp. 121–125, Jan. 2018. [Online]. Available: https://www.sciencedirect.com/science/article/pii/S1359646217305067
[31] V. B. Biscuola and M. A. Martorano, "Mechanical blocking mechanism for the columnar to equiaxed transition," *Metall. Mater. Trans. A*, vol. 39, no. 12, pp. 2885–2895, Dec. 2008.
[32] E. Pošković, F. Franchini, L. Ferraris, F. Carosio, and M. A. Grande, "Rapid characterization method for SMC materials for a preliminary selection," *Appl. Sci.*, vol. 11, no. 24, p. 12133, Dec. 2021. [Online]. Available: https://www.mdpi.com/2076-3417/11/24/12133
[33] E. Poškovic, F. Franchini, and L. Ferraris, "The magnetization effect on soft magnetic composite prepared stators of axial flux motors," in *Proc. IEEE Energy Convers. Congr. Expo. (ECCE)*, Oct. 2022, pp. 1–7.

MICHELE QUERCIO (Member, IEEE) was born in Avola, Italy, in 1994. He received the bachelor's and master's degrees in mechanical engineering from Politecnico di Torino, Turin, Italy, in 2016 and 2018, respectively, where he is currently pursuing the Ph.D. degree in electrical engineering with the Energy Department, with a focus on computation of electromagnetic fields, design of magnetic shields, implementation of computational algorithms, and renewable energy. He is also an actually Convenor of the working group on non-destructive testing applied to the additive manufacturing sector of the Italian National Association of Non Destructive Testing and a Vice-Convenor of the same commission WG6 (https://www.efndt.org/Organisation/Working-Groups/Working-Group-6-NDT-in-Additive-Manufacturing) of the European Federation for Non Destructive Testing (EFNDT).

FRANCESCO GALBUSERA was born in Lecco, Italy, in 1995. He received the bachelor's and master's degrees in mechanical engineering from Politecnico di Milano, Italy, in 2018 and 2020, respectively, where he is currently pursuing the Ph.D. degree in mechanical engineering, with a focus on novel LPBF processing techniques to enhance the processability of e-mobility alloys.

EMIR POSKOVIC was born in Sarajevo, Bosnia and Herzegovina. He received the B.S. and M.Sc. degrees in electrical engineering from Politecnico di Torino, in 2006 and 2008, respectively, and the Ph.D. degree in electrical energy engineering from the University of Padova, in 2020. He is currently an Assistant Professor with the Energy Department, Politecnico di Torino, and a Key Researcher with the Magnetic Characterization Laboratory, Alessandria campus, Politecnico di Torino. His research interests include soft and hard magnetic materials, electrical machines, alternative, and renewable energy (micro-hydro, fuel cell, and PV-photovoltaic).

FAUSTO FRANCHINI received the B.S. degree in electrical engineering from Politecnico di Torino, Alessandria, Italy, in 2003. Since 2004, he has been a Technician with the Electrical Engineering Laboratory, Politecnico di Torino, Turin, Italy, where he has been responsible of the Laboratory, since 2007. His research interests include electromagnetic metrology, electromagnetic compatibility, data acquisition, control, and automation.

LUCA FERRARIS received the M.S. degree in electrical engineering from Politecnico di Torino, Turin, Italy, in 1992. In 1995, he joined the Department of Electrical Engineering, Politecnico di Torino, where he is currently an Associate Professor of electrical machines and drives and also coordinates the experimental activities of Electric and Electromagnetic Laboratories. He has published more than 120 technical papers in conference proceedings and technical journals. His research interests include the energetic behaviour of machines, innovative magnetic materials for electromagnetic devices, electrical traction, electromagnetic compatibility, and renewable energies.

ALDO CANOVA was born in Biella, Italy, in 1967. He received the Laurea and Ph.D. degrees in electrical engineering from Politecnico di Torino, Turin, Italy, in 1992 and 1996, respectively. In 1995, he became a Researcher, then in 2003, an Associate Professor, and finally in 2017, a Full Professor with the Energy Department "Galileo Ferraris," Politecnico di Torino. He has authored/coauthored about 180 scientific publications in international conference proceedings and international journals and invented eight patents. He is involved in research activities related to the numerical computation of electromagnetic fields in the area of power devices and magnetic shielding, energy system modeling and optimization, and non destructive testing. He has been a member of Comitato Elettrotecnico Nazionale (CEI) serving on Technical Committee CT106 (methods for the assessment of electric, magnetic and electromagnetic fields associated with human exposure), since 2004. He is also an actually General Secretary of the Italian National Association of Non Destructive Testing.

GIAMBATTISTA GRUOSSO (Senior Member, IEEE) was born in 1973. He received the B.S., M.S., and Ph.D. degrees in electrical engineering from Politecnico di Torino, Italy, in 1999 and 2003, respectively. From 2002 to 2011, he was an Assistant Professor with the Department of Electronics and Informatics, Politecnico di Milano, where he has been an Associate Professor, since 2011. He is the author of more than 80 papers on journals and conferences on the topics. His research interests include electrical engineering, electronic engineering, industrial engineering, electrical vehicles transportation electrification, electrical power systems optimization, simulation of electrical systems, digital twins for smart mobility, factory and city, and how they can be obtained from data.

ALI GOKHAN DEMIR was born in Istanbul, Turkey, in 1985. He received the Ph.D. degree in mechanical engineering from Politecnico di Milano, in collaboration with the University of Cambridge gaining a European Ph.D. title, in 2014. He has been an Associate Professor with the Department of Mechanical Engineering, Politecnico di Milano, since 2021. His current research interests include laser-based manufacturing processes, mainly, additive manufacturing, laser micromachining, and laser welding. Within his research, he gives emphasis to the light-material interaction mechanism in temporal, spatial, and wavelength domains to gather a greater understanding of both existing and new processes.

BARBARA PREVITALI received the Ph.D. degree in manufacturing and production system from Politecnico di Milano, in 2002. In 2016, she was a Full Professor with the Mechanical Engineering Department, Politecnico di Milano. She leads the SITEC Laboratory for Laser Applications and PromozioneL@ser, AITeM, which collects Italian laser users in industry and academia. Her current research interests include modeling, optimization, and control of laser processes in their application in various fields. On these research subjects, she has authored or coauthored over 100 papers in refereed international journals and international conferences and several international patents.

Open Access funding provided by 'Politecnico di Torino' within the CRUI CARE Agreement